International Journal of Coal Geology 265 (2023) 104165

Contents lists available at ScienceDirect

International Journal of Coal Geology

journal homepage: www.elsevier.com/locate/coal

Origin and geochemical significance of antimony in Chinese coal

Xinyu Li [a,b], Guangyi Sun [a,*], Yunjie Wu [a,c], Mengying Zhou [a,c], Zhonggen Li [d], Xiangyang Bi [c], Jen-How Huang [a], Xinbin Feng [a,*]

[a] State Key Laboratory of Environmental Geochemistry, Institute of Geochemistry, Chinese Academy of Sciences, Guiyang 550081, China
[b] University of Chinese Academy of Sciences, Beijing 100049, China
[c] State Key Laboratory of Biogeology and Environmental Geology, School of Earth Sciences, China University of Geosciences, Wuhan 430074, China
[d] School of Resources and Environment, Zunyi Normal College, Zunyi 563006, China

ARTICLE INFO

Keywords:
Coal
Antimony isotopes
Antimony source
Geochemical tracer
Isotopic fractionation
Trace elements

ABSTRACT

A total of 159 coal samples from different regions, periods and ranks across China were systematically analyzed for antimony (Sb) isotopic composition (ε^{123}Sb), trace element contents and total sulfur content (TS) in this study. Here, we discuss the origin of Sb in coal from different regions of China. Antimony in coal from SW and NE China is primarily of hydrothermal fluid and leachate origins, respectively. In comparison, Sb in northern Chinese coal mainly comes from terrigenous materials and hydrothermal fluid. Antimony in coal from NW China may be influenced by the superposition of hydrothermal activity and leaching solution. Inorganic minerals (e.g., sulfide) and organic matter in coal are the determining factors for Sb enrichment in coal. The Sb isotopic fingerprint of Chinese coal is 2.46 ± 1.01 ε (weighted mean ± 1 SD, ranging from −4.45 to +9.72 ε). Accordingly, the isotopic composition of Sb in coal has great potential not only for researching Sb isotope fractionation in hydrothermal systems but also for tracing Sb release and transport in the supergene eco-environment. Furthermore, the establishment of Sb isotopic fingerprint for coal could largely reduce the uncertainty in the application of Sb isotope methods.

1. Introduction

Antimony (Sb) is a metalloid that has been listed as a strategic resource by many countries or international organizations due to its indispensable industrial applications (Krenev et al., 2015). On the other hand, Sb pollution has posed a serious threat to the supergene ecosystem (Filella et al., 2002; He et al., 2019; He et al., 2012). Global atmospheric Sb emissions from coal combustion accounted for 73.4% (803 tons) of the total anthropogenic atmospheric Sb emissions in 2010 (Tian et al., 2014). According to projections from current environmental protection laws, even by 2050, atmospheric Sb emissions from coal combustion will still account for 29.6% (447 tons) of China's total anthropogenic atmospheric Sb emissions. (Zhou et al., 2015). China is the world's largest producer and consumer of coal, and coal production and consumption were responsible for 47.6% and 52.9% of global coal production and consumption in 2019, respectively (BP, 2020; Nation Bureau of Statistics of China, 2021). In addition, there is Sb-rich coal in several regions of China with a higher potential environmental risk. For instance, the total Sb content (TSb) in some coals from Xingren, Guizhou (up to 3,860 mg/kg) (Dai et al., 2006), Shengli Coalfield, Inner Mongolia (up to 348 mg/kg) (Qi et al., 2007), and Baise, Guangxi (up to 77 mg/kg) (Yan et al., 2019) are at least 2 orders of magnitude higher than the average TSb in coal nationwide (0.84 mg/kg) (Dai et al., 2012a) and worldwide (0.84–1.00 mg/kg) (Ketris and Yudovich, 2009).

Trace elements in coal provide geologic information about the sedimentary environment and tectonic history, as they are geochemically characterized by the accumulation of terrigenous materials and coal-forming plants, as well as the interaction between regional hydrothermal fluid and leaching processes (Dai et al., 2021; Dai et al., 2012a). In the case of Sb in coal, previous studies have mostly noted the spatial distribution of Sb content and the way in which Sb occurs in coal. Namely, these are directly related to the environmental risks caused by the release of Sb during coal combustion (Dai et al., 2021; Dai et al., 2020; Qi et al., 2008). Nonetheless, comprehensively understanding the occurrence mode of Sb in coal is still challenging today, since the recovery of total Sb from coal with chemical extraction never exceeded 70% (Finkelman et al., 2018). Studies of the Sb origin could provide a better understanding of the occurrence mode of Sb in coal (Dai et al.,

* Corresponding author.
E-mail addresses: sunguangyi@mail.gyig.ac.cn (G. Sun), fengxinbin@vip.skleg.cn (X. Feng).

https://doi.org/10.1016/j.coal.2022.104165
Received 7 September 2022; Received in revised form 3 December 2022; Accepted 7 December 2022
Available online 9 December 2022

2012a). Song et al. (2018) reported that Sb in coal from the Laoheishan Basin, Heilongjiang, NE China, is predominantly present in pyrite and that sedimentary input could be the source. Antimony in coal from the Shengli Coalfield, Inner Mongolia, N China, is also associated with pyrite, and its origin seems related to hydrothermal activity (Dai et al., 2012b) and leaching solution (Qi et al., 2007). In comparison, Sb in coal from Shimenkan, Xingren, Guizhou, SW China is derived from low-temperature hydrothermal fluid (Dai et al., 2006). In Ge-rich coal from the Pavlovka brown coal deposit, Khankai Massif, Russia, Sb is mainly bound to organic matter, which is associated with a mixed solution of groundwater and volcanic hydrothermal fluid (Seredin, 2003). Antimony in coal from Balingian, Sarawak, Malaysia is linked to mineralized terrigenous materials (Sia and Abdullah, 2012). The aforementioned studies are mainly based on petrography observations or element content characteristics in coal. More direct evidence is essential to elucidate the origin of Sb in coal (Dai et al., 2005; Qi et al., 2008; Qi et al., 2007; Seredin, 2003; Sia and Abdullah, 2012; Song et al., 2018). Nevertheless, comprehensive investigations concerning the source of Sb in coal are lacking to date to draw any solid conclusion. Therefore, it is necessary to use more reliable methods and direct evidence to comprehensively constrain the origin of Sb in Chinese coal.

Non-traditional stable isotopes are widely used in geology, environmental science and other fields because of their significant diversity in different natural media and unique fingerprints (Teng et al., 2017). The application of non-traditional stable isotopes to coal includes the study of the origin of elements, revealing the geochemical processes involved in the formation of coal, and tracing sources of pollutants. For example, the isotopic composition of mercury (Hg) in coal has been shown to be a powerful indicator for revealing the source of Hg in coal, inferring the process of coalification and tracking Hg pollution from coal combustion (Sun et al., 2014; Sun et al., 2016; Yin et al., 2014). Strontium (Sr) isotopes not only reveal the mode of formation of the coal-hosted germanium (Ge) deposit but also provide an indication for the hydrological pathways of the mineralizing fluid (Liu et al., 2021a; Spiro et al., 2019).

Antimony has two stable isotopes, ^{121}Sb (57.21%) and ^{123}Sb (42.79%). The high-precision measurement of Sb isotopes has recently been achieved based on the use of multiple-collector inductively coupled plasma–mass spectrometry (MC–ICP–MS). Additionally, Sb isotope methods have potential applications in a variety of geological and environmental contexts (Liu et al., 2021a; Sun et al., 2021). For instance, Sb isotopes have been used to reveal the origin and formation mechanism of metallogenetic elements in mineralization (Wang et al., 2021; Zhai et al., 2021). Moreover, different degrees of Sb isotope fractionation have been evidenced in the natural redox reactions, mineral adsorption and precipitation of hydrothermal fluid. (Rouxel et al., 2003; Zhai et al., 2021; Zhou et al., 2022). Since coal is an important host for geological records and a major source of anthropogenic Sb emissions, it is crucial to accurately determine the Sb isotopic fingerprint of coal to reveal the geological Sb origin and trace environmental Sb.

China is rich in coal resources, and coal-forming basins are widely distributed, covering SW, NE, N, and NW China. Based on the coal geology and coalfield distribution in China, six major coal-forming periods have been classified (Ren et al., 2006), including late Carboniferous and Early Permian (C_2–P_1), Late Permian (P_2), Late Triassic (T_3), Early and Middle Jurassic (J_{1-2}), Late Jurassic and Early Cretaceous (J_3–K_1), and Paleogene and Neogene (E–N). In addition, there are differences in the coal-forming environment in China. The coal in P_2 from SW China was formed in a restricted carbonate platform and influenced by seawater (Dai et al., 2013; Shao et al., 1998). While, the coal from other regions in China was formed in the continental environment, such as lakes, deltas and alluvial fans (China National Administration of Coal Geology, 2016; Li et al., 2017). The spatial and temporal variation in Chinese coals encompasses the possible diversity of Sb sources in coal, which facilitates a more comprehensive understanding of the environmental geochemistry of Sb in coal. In the present study, we systematically collected coal samples from major coal-forming basins across China, analyzed TSb, Sb isotopic compositions, major and trace element contents, TS, and ash yields in coal, and integrated petrographic characteristics and isotopic data of Hg and S (Δ^{199}Hg and δ^{34}S) in coal to reveal the origin of Sb in coal by region. At the same time, a database of the Sb isotopic fingerprint of coal in China has been established to provide basic data support for tracing geological Sb sources and environmental Sb pollutants.

2. Methodology

2.1. Sample collection and analysis

In this study, 159 coal samples were collected from 16 different coal-producing provinces, one sample from each site, covering almost all large coal-forming basins in China (Fig. S1). In addition, the regional differences in coal reserves and TSb in coal are fully considered in determining the distribution of sample sizes to reduce uncertainty in the results. For example, more samples were collected from provinces with large coal reserves or with high rates of Sb anomalies in coal. Stockpile random sampling and loader random sampling were used to collect coal samples from the bunkers. For coal mine sampling, we took twenty subsamples of fresh coal and mixed them together to make one valid sample. The basis for the selection of sampling sites, the distribution of the number of different areas and detailed sampling methods are shown in the Supporting Information (SI) and Table S1. The coal samples were air-dried, ground (< 0.150 mm) by vibratory disc mills, and stored in polyethylene self-sealing bags for preservation.

All reagents used in the experiment and relevant information are listed in Table S2. The total sulfur content (TS) of the coal samples was measured using an automatic sulfur analyzer (ASA, LC–S–700, Lichen Technology, China) based on the coulometric titration method (GB/T214–2007, 2007), which is detailed in SI. The analysis of ash yield and coal rank classification are based on the American Society of Testing Materials (ASTM) method (ASTM, 2020, 2021). The coal samples were digested with customized high-pressure bombs following the modified processes reported in Zhu et al. (2018) and Wu et al. (2020). Total Sb in the digestion solution was determined using hydride generation–atomic fluorescence spectrometry (HG–AFS, AFS–8520, Beijing Haiguang, China) with a detection limit of 0.05 ng/mL. Information regarding the digestion and analysis is detailed in the SI. The major and trace elements in the digestion solution were quantified using ICP–OES (Wasst-mpx, USA) and ICP–MS (Agilent 7500, USA), respectively. According to Sun et al. (2021), the digestion solution was pretreated for Sb isotopic analysis with MC–ICP–MS using a two-step chromatographic purification process (detailed in SI (Table S3)). The antimony isotopic composition of the samples is reported as ε^{123}Sb in per mil (ε):

$$\varepsilon^{123}\mathrm{Sb} = \left[\frac{\left(^{123}\mathrm{Sb}/^{121}\mathrm{Sb}\right)_{\mathrm{sample}}}{\left(^{123}\mathrm{Sb}/^{121}\mathrm{Sb}\right)_{\mathrm{standard}}} - 1\right] \times 10{,}000 \quad (1)$$

Antimony-containing solution produced by the National Institute of Standards and Technology, U.S. (NIST SRM 3102a) was chosen as the reference standard for Sb isotopic analysis. The sample-standard bracketing method and element doping (SSB-ED) were used to control instrumental error, with an accuracy of 0.4 ε (2SD).

2.2. Quality assurance and quality control

The experimental conditions and processing of experimental materials are described in detail in the SI. In the case of TS, certified reference materials (CRM) of anthracite (GSB06–3345-2006 [ZBM123]) and bituminous coal (GBW 11108 L) were used, with recoveries of TS from the aforementioned CRM between 96–102 %. Certified reference material of bituminous coal (NIST SRM 1632d) and duplicate and blank

samples were used for quality assurance and quality control during the digestion process. The recoveries of Sb from the CRM and duplicate samples ranged from 94 to 102 %. The TSb in the blank samples was below the detection limit of HG–AFS (0.05 ng/mL). The recoveries of other trace elements in CRM ranged between 90–115 %. For Sb isotopic analysis, the digestion solution of NIST SRM 1632d and the Sb standard solution from SPEX Certiprep (IGCAS-SPEX) were processed by chromatographic purification and then measured with MC–ICP–MS. The antimony isotopic composition of CRM in this study is in good agreement with the published data (Table S4) (Sun et al., 2021).

3. Results and discussion

3.1. Geochemistry of coals

In 159 coal samples in this study, the TS ranges from 0.10 to 8.12 % (Table S1). Coal from SW China has a higher TS than that from the other regions (Fig. S2). The TSb ranges from 0.08 to 4.51 mg/kg (Figs. 1a and Table S1), with a lognormal distribution (Fig. S3a). The arithmetic mean and median of TSb were 0.66 ± 0.74 mg/kg (mean ± standard deviation [1SD], N = 159) and 0.42 ± 0.47 mg/kg (median ± median absolute deviation, N = 159), respectively. To reduce the impact of regional TSb differences and more accurately assess the overall TSb in coal from China, we calculated the weighted average of TSb using coal reserves in each Chinese province (Eq. S1, Table S5). The weighted mean of TSb in coal from China is 0.66 ± 0.65 mg/kg (1SD). Compared with TSb in coal worldwide and the Clarke value of geological samples shown in Table S6, TSb in this study is slightly lower than that in coal worldwide (0.92 mg/kg) and from China (0.71–1.30 mg/kg) published previously (Bai et al., 2007; Dai et al., 2012a; Ketris and Yudovich, 2009; Ren et al., 2006; Tang and Huang, 2004). As a sediment rock, coal from China has more enriched TSb relative to the upper continental crust (UCC, 0.2 mg/kg) (Taylor and McLennan, 1995). Nevertheless, its TSb is lower than that of sedimentary rock (1.2 mg/kg) (Ronov et al., 1990). The value of ε^{123}Sb in the analyzed coal exhibits a normal distribution based on the Shapiro–Wilk normality test with an arithmetic mean of 2.47 ± 1.58 ε (1SD, N = 159) and a range of −4.45 to +9.72 ε (Fig. S3b). This indicates strong isotopic fractionation (14.17 ε) between coal from different regions in China. Based on Eq. S2 in the SI, the weighted mean of ε^{123}Sb in Chinese coal is 2.46 ± 1.01 ε (1SD, Table S5).

3.2. Effects of periods, coal ranks, and spatial distribution

With respect to the different coal-forming periods (Fig. 2a), TSb in coal from J_3–K_1 (0.90 ± 0.97 mg/kg, 1SD) and P_2 (0.55 ± 0.57 mg/kg, 1SD) is significantly higher ($p < 0.01$, *t*-test) than that from J_{1-2} (0.37 ± 0.45 mg/kg, 1SD), E–N (0.37 ± 0.16 mg/kg, 1SD), and C_2–P_1 (0.28 ± 0.17 mg/kg, 1SD). However, there is no significant difference ($p > 0.05$, *t*-test) between the ε^{123}Sb in coal from C_2-P_1 (2.75 ± 1.08 ε, 1SD), J_{1-2} (2.63 ± 0.97 ε, 1SD), J_3-K_1 (2.95 ± 0.72 ε, 1SD), and E–N (2.31 ± 0.66 ε, 1SD). The ε^{123}Sb of coal in P_2 is more negative (1.87 ± 2.37 ε, 1SD, $p < 0.05$, *t*-test) than that of coal in other periods, which is related to the large negative fluctuation of ε^{123}Sb in P_2 coal from Guizhou Province (Fig. 1b).

In this study, anthracites and bituminous coals are observed in C_2–P_1, P_2, and J_{1-2}, whereas subbituminous coals and lignites are found in all coal-forming periods (C_2–P_1, P_2, J_{1-2}, J_3–K_1, and E–N, Table S1), which is in line with the trend of increasing coal maturity over time (China National Administration of Coal Geology, 2016). In anthracites, TSb (0.25 ± 0.35 mg/kg, 1SD) is significantly lower ($p < 0.01$, *t*-test) than in bituminous coals (0.41 ± 0.60 mg/kg, 1SD), subbituminous coals (0.49 ± 0.46 mg/kg, 1SD), and lignites (0.47 ± 0.31 mg/kg, 1SD), suggesting that anthracites with a high maturity may contain fewer impurities than other coal types (Fig. 2b). However, the difference in ε^{123}Sb between different coal ranks is insignificant ($p > 0.05$, *t*-test).

The antimony isotopic composition and TSb in coal from different regions of China vary significantly (Figs. 1 and 3). Based on TSb, ε^{123}Sb, TS, and coal-formation periods in this study, four distinct regions can be categorized: SW China (region A), NE China (region B), N China (region C), and NW China (region D). SW China mainly comprises P_2 coal, with high TSb (0.82 ± 0.88 mg/kg, 1SD, maximum of 4.51 mg/kg), a wide range of ε^{123}Sb (−4.45 to +9.72 ε), and high TS (3.15 ± 2.10 %, 1SD). NE China has a long coal-forming period, including C_2–P_1, J_{1-2}, J_3–K_1, and E–N. Coal from this region also has high TSb (0.84 ± 0.90 mg/kg, 1SD, maximum of 4.14 mg/kg), but TS is only 0.66 ± 0.48 % (1SD) and ε^{123}Sb is 2.57 ± 0.85 ε (1SD, ranging from −0.21 to +4.23 ε). The coal-forming periods in N and NW China are C_2–P_1 and J_{1-2}, respectively. They have similar low TSb (0.42 ± 0.22 mg/kg for N China, 0.48 ± 0.56 mg/kg for NW China, 1SD), low TS (1.01 ± 1.28 % for N China, 0.84 ± 0.85 % for NW China, 1SD), and narrow ε^{123}Sb values (2.65 ± 1.15 ε for N China, ranging from 0.47 to 6.87 ε; 2.77 ± 0.93 ε for NW China, ranging from 0.67 to 6.64 ε) (Figs. 1, 3 and S2).

Coal from SW China and NE China can be distinguished from coal from N China and NW China (Fig. 4). SW and NE China both have coal

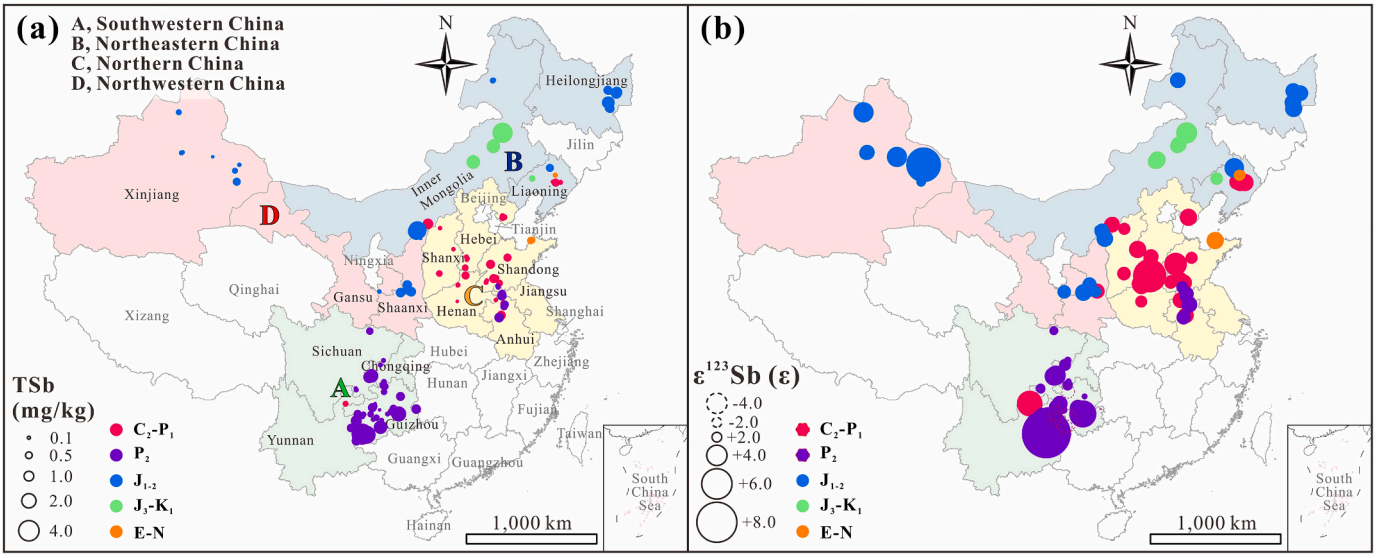

Fig. 1. (a) The total antimony content (TSb) and (b) ε^{123}Sb in coal from different regions in China. TSb and ε^{123}Sb are represented as circles of different sizes.

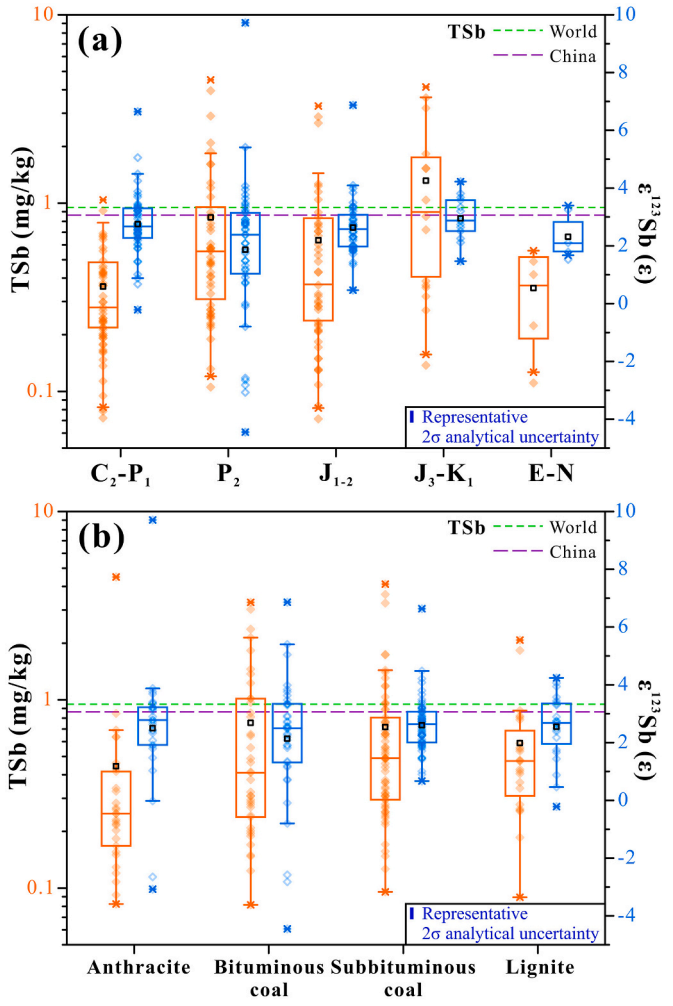

Fig. 2. Variations of TSb and ε^{123}Sb in coal categorized on the basis of (a) the coal-forming period and (b) coal rank. The box shows the central 50 % (25th–75th percentile) data with the median (50th percentile) value shown as the horizontal line inside the box. The box height (difference between the lower and upper quartiles) is defined as the interquartile range (IQR). The whisker represents the range of −1.5 IQR to +1.5 IQR, and data outside of this range are outliers. The mean value is shown as a square symbol.

with higher TSb ($p < 0.01$, *t*-test). In particular, SW China has a wider range of ε^{123}Sb (−4.45 to +9.72 ε). Based on the concentration coefficient (CC) of Sb in coal (Dai et al., 2012a; Ketris and Yudovich, 2009), the enrichment of Sb occurred in coal from SW and NE China, formed in P^2, $J_{1–2}$, and J_3-K_1, and ranked as bituminous and subbituminous coal (Fig. S4). Thus, the Sb-rich coal can be divided into P_2 coal from SW China and J_1-K_1 coal from NE China.

3.3. Origin of Sb in coal

There are significant regional differences in the coal-forming periods and depositional environments of Chinese coal (Li et al., 2017), as reflected in the geochemical characteristics of the coal (such as TSb, Sb isotopic composition, and TS). This further suggests that the different sources of Sb in coal vary from region to region. Therefore, the origins of Sb in Chinese coal are discussed separately on an aforementioned regional basis, i.e., SW China (region A), NE China (region B), N China (region C), and NW China (region D) (Fig. 1). In this study, the sedimentary environment, petrographic characteristics, isotopic composition, element content and previous studies of coal are comprehensively integrated to discuss and constrain the origin of Sb in coal from China.

3.3.1. Southwestern China (region A)

The coal-forming environment of P_2 in SW China is different from that in other regions due to strong marine influences (China National Administration of Coal Geology, 2016; Dai et al., 2013; Li et al., 2017; Shao et al., 1998), so the ocean could be one of the sources of Sb in coal. However, a marine source of Sb in sedimentary periods of coal could be ruled out according to (1) the sea water has a narrow range of ε^{123}Sb (no significant difference based on mean ± 1SD for the surface [4.40 ± 0.40 ε] and the deep [4.28 ± 0.47 ε] ocean), which is significantly different from the wide range of ε^{123}Sb in coal from SW China (−4.45 to +9.72 ε); and (2) the even and low TSb in sea water (0.16–0.17 ng/mL) is not conducive to the formation of Sb-rich coal in this area (Cutter and Cutter, 1998; Rouxel et al., 2003). On the basis of Sb isotopic composition, hydrothermal fluid may be the source of Sb in coal. Namely, ε^{123}Sb in coal from SW China (−4.45 to +9.72 ε) is similar to that in ore-forming hydrothermal fluid (−2.7 to +8.6 ε) (Zhai et al., 2021). Black shale, which is widely distributed in SW China, contains a large quantity of trace elements (TSb = 1.0 to 34.3 mg/kg) (Zhang et al., 2020). The black shale provides the material basis for Sb enrichment in hydrothermal fluid, leading to the formation of Sb mines in Guizhou Province during the post-sedimentary period of coal, such as the Qinglong and Dushan Sb mines (Hu et al., 2020; Zhang et al., 2020). Coincidentally, the Sb-rich coal has good geographical overlap with the Qinglong Sb mine (Fig. S5). Epigenetic pyrite is additional evidence indicating that coal underwent hydrothermal activity (Fig. S6a) (Liu et al., 2021a). In addition, the Hg mass-independent fractionation (MIF) in coal affected by hydrothermal fluid has a characteristic Δ^{199}Hg ≈ 0 ‰ because there is no photoreduction process that can lead to MIF (Sun et al., 2014). The Δ^{199}Hg in coal from Guizhou, Sichuan, and Chongqing is ~0 ‰ (Fig. 5a), indicating that the coal from SW China was affected by hydrothermal fluid (Biswas et al., 2008; Sun et al., 2014; Yin et al., 2014). For the trace elements, TSb correlates significantly and positively with the arsenic (As) content in coal from SW China ($R^2 = 0.86$, $p < 0.01$, *t*-test) but with a stronger correlation ($R^2 = 0.95$) in coal specifically from Guizhou Province (Fig. 6a). The As content of the low-rank coals is considerably lower than that in bituminous coal, indicating that epigenetic As accounts for the main part (Finkelman et al., 2018). The majority of As exists in the form of sulfide (arsenopyrite) in coal and was introduced to the coal by hydrothermal fluid in the postsedimentary period (Dai et al., 2021; Finkelman et al., 2018; Tian et al., 2015; Zheng et al., 1999). Dai et al. (2006) also reported that Sb in coal seams from the Guizhou region mainly originates from Sb-rich low-temperature hydrothermal fluid.

The sulfide mineral in coal is considered one of the most important factors controlling Sb in coal (Dai et al., 2021; Finkelman et al., 2018), and TS in coal from SW China is significantly higher than that in coal deposited in terrestrial environments from the other three regions (Fig. S2) (Li et al., 2017). Although a weak correlation between TS and TSb is observed in coal from SW China ($R^2 = 0.02$, $p = 0.19$, *t*-test, Fig. S7), significant correlations are seen between TSb/TS × 10,000 and TSb (Fig. 7a). Moreover, the regression slope differs notably between high-sulfur coal (TS ≥ 2%, $R^2 = 0.86$, $p < 0.01$, *t*-test) and non-high-sulfur coal (TS < 2%, $R^2 = 0.46$, $p < 0.01$, *t*-test) (Fig. 7a). In addition, a wide range of ε^{123}Sb (−4.45 to +9.72 ε) is also observed in coal with a high TS from P_2 (Fig. 7b), mirroring that sulfur may be one of the important factors controlling TSb in coal from SW China. The intervention of seawater is more conducive to the enrichment of sulfur in coal because sulfate in seawater was reduced to H_2S under the action of microorganisms in the sediment (Berner, 1984). The reducing environment caused by seawater also benefits the formation of Fe^{2+}, which promotes the formation of pyrite in sediments (Chou, 2012; Hu et al., 2005; Tang et al., 2000). The transgression during the coal-forming period resulted in δ^{34}S in coal being close to that of the sulfide in marine sediment (δ^{34}S = −22 to +10 ‰), which is related to the preferential reduction of light sulfur isotopes by microorganisms, leading to more negative δ^{34}S (−50 to +20 ‰) (Nehlich, 2015; Seal, 2006; Xiao

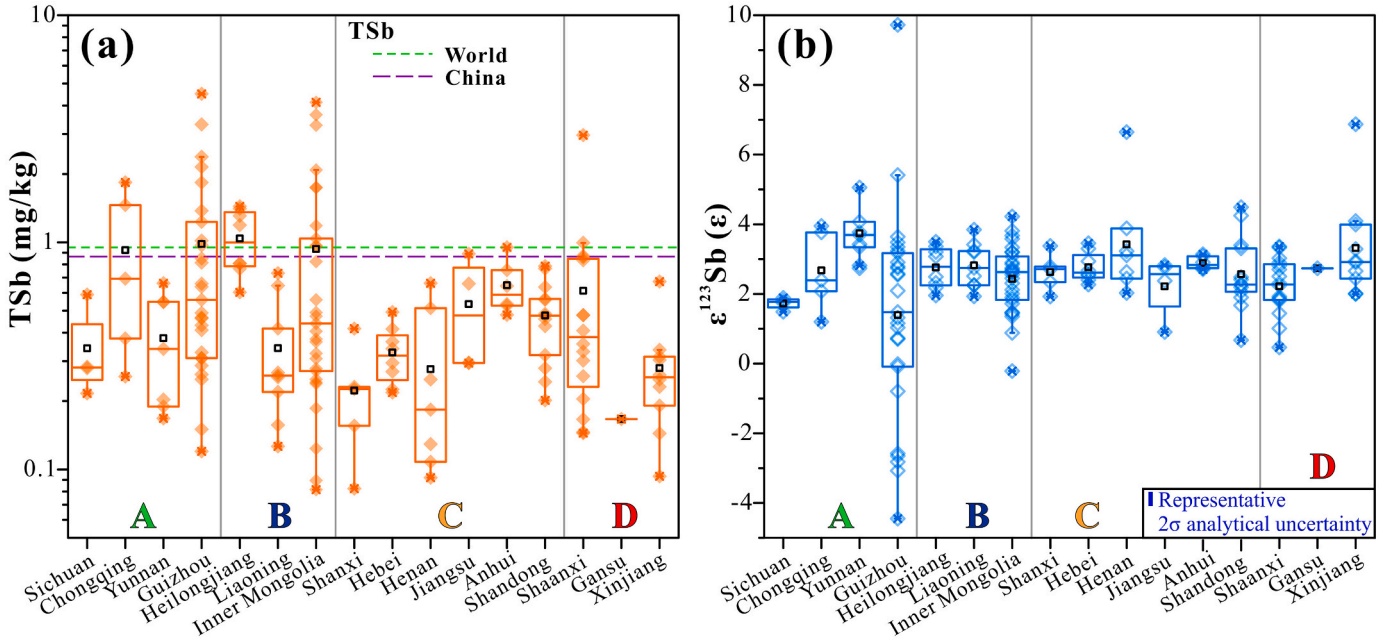

Fig. 3. Variations of (a) TSb and (b) ε^{123}Sb in coal categorized on the basis of geographic location (region A, SW China; B, NE China; C, N China; and D, NW China). The box shows the central 50 % (25th–75th percentile) data with the median (50th percentile) value shown as the horizontal line inside the box. The box height (difference between the lower and upper quartiles) is defined as the interquartile range (IQR). The whisker represents the range of −1.5 IQR to +1.5 IQR, and data outside of this range are outliers. The mean value is shown as a square symbol.

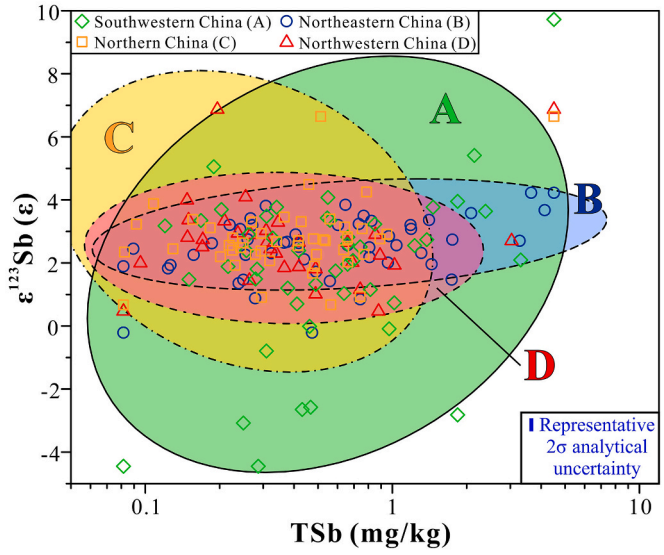

Fig. 4. Discrimination diagram of TSb vs. ε^{123}Sb for Chinese coal based on the coal spatial distribution (ellipses are plotted based on the range of 95 % confidence intervals).

and Liu, 2011). Coal from SW China ($\delta^{34}S = -7.52 \pm 2.46$ ‰ for Guizhou, 1SD, N = 18; $\delta^{34}S \approx 0$ ‰ for Sichuan, Chongqing, and Yunnan) has a significantly lighter $\delta^{34}S$ than coal formed in continental environments from other Chinese regions (Fig. 5b) (Hong et al., 1992; Xiao et al., 2011). In addition, the $\delta^{34}S$ in coal from SW China is similar to that in sulfides in marine sediments (Fig. 5b). In particular, the $\delta^{34}S$ in coal from Guizhou Province, which has the largest coal reserve and the highest TS in coal from SW China, is lower than the $\delta^{34}S$ of plants ($\delta^{34}S = -1.5$‰) and hydrothermal sulfide deposits (most $\delta^{34}S > 0$‰) (Seal, 2006; Tryst and Fry, 1992; Zhang and Gu, 1996). Therefore, the $\delta^{34}S$ in coal proves that seawater is the major source of sulfur in coal from SW China. Since sulfur occurs mainly as pyrite in sulfur-rich coal from China (Ni, 1997; Xiao and Liu, 2011), most sulfides found in sulfur-rich coal from SW China are supposed to be pyrite. Petrographic and mineralogical studies of coal indicated that pyrite in coal formed under the influence of seawater is mainly in the form of granular and framboidal particles (Tang et al., 2000). Most of the pyrite in coal from SW China has been found in the form of individual particles or framboidal particles (Fig. S6b, c, d), indicating that pyrite in coal from SW China was formed during the sedimentary period of coal (i.e., P_2) (Dai et al., 2015b; Liu et al., 2021a; Xie et al., 2016), which is earlier than the activity period of regional Sb-bearing hydrothermal fluid (the hydrothermal Sb deposits in South China were formed in 93–148 Ma in the Mesozoic) (Peng et al., 2003; Zhang et al., 2020). Antimony easily forms covalent bonds with sulfur due to its electronic layer structure, which leads to the strong affinity between Sb and sulfide in geochemical processes (White, 2013). Fissure-filled stibnite was observed in Sb-rich coal by SEM, which indicates that the Sb in coal is of epigenetic hydrothermal origin (Karayiğit et al., 2000). Antimony in coal is generally present in the solid solution of pyrite and other accessory sulfide minerals (e.g., stibnite and getchellite) (Dai et al., 2021; Dai et al., 2006; Finkelman, 1994). Therefore, it is possible that Sb in the hydrothermal fluid was fixed by the sulfide in coal during the post-sedimentary periods of coal. Moreover, this genetic model is also consistent with the weak correlation between TSb and TS (Fig. S7). Such a correlation could become insignificant in high-sulfur coal without the influence of the regional Sb-bearing hydrothermal fluid. These two correlations based on TS in coal (Fig. 7a) suggest that sulfur enrichment is a prerequisite for the formation of Sb-rich coals. Accordingly, we propose that the origin of Sb in coal from SW China is Sb-bearing hydrothermal fluid, which was immobilized by syngeneic sulfides (pyrite) in coal during the postsedimentary period (Fig. 8a). The hydrothermal fluid origin of Sb in coal from SW China is further confirmed by the similar range of Sb isotopic composition (ε^{123}Sb = −4.45 to +9.72 ε) in coal to that in hydrothermal fluid (ε^{123}Sb = −2.7 to +8.6 ε) but differs from that in sea water (ε^{123}Sb = 4.40 ± 0.40 ε).

3.3.2. *Northeastern China (region B)*

The small range of ε^{123}Sb (−0.21 to +4.23 ε) and the negative Δ^{199}Hg (ranging from −0.05 ‰ to −0.24 ‰, Fig. 5a) rule out the

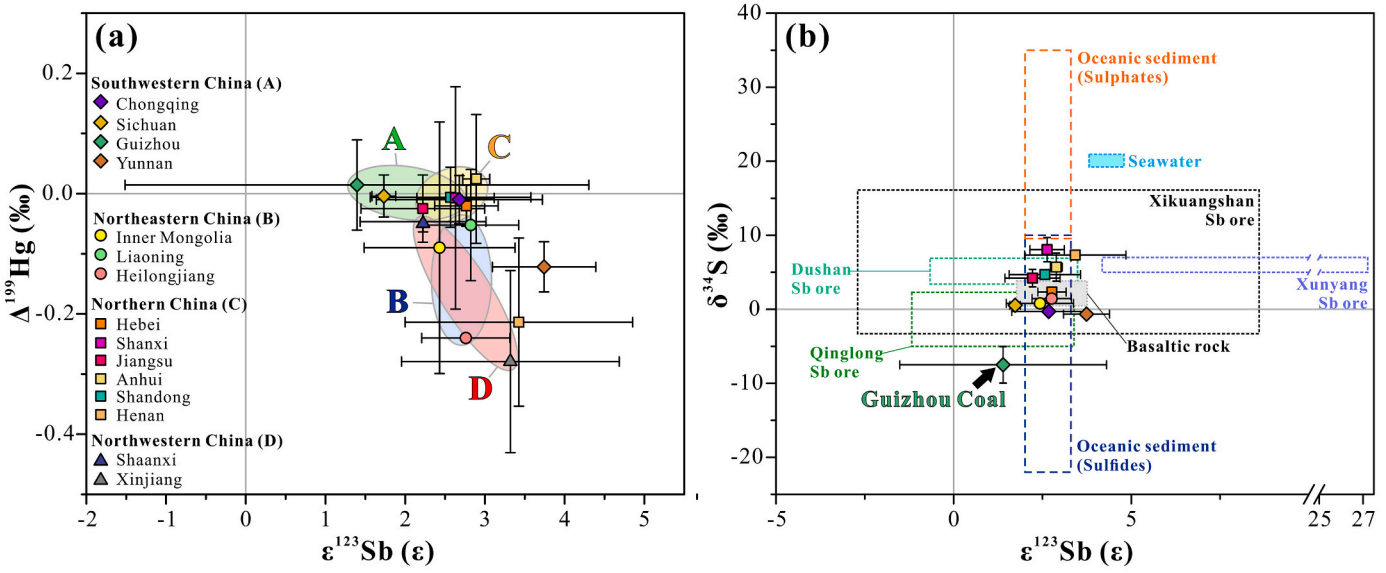

Fig. 5. Discrimination diagram of (a) $\varepsilon^{123}Sb$ vs. $\Delta^{199}Hg$ and (b) $\varepsilon^{123}Sb$ vs. $\delta^{34}S$ in coal from different regions in China. Error bars represent 1SD for $\varepsilon^{123}Sb$, $\Delta^{199}Hg$, and $\delta^{34}S$. Dashed lines represent the range of $\varepsilon^{123}Sb$ and $\delta^{34}S$. Data regarding $\delta^{34}S$, $\Delta^{199}Hg$, and $\varepsilon^{123}Sb$ are gathered from Tables S7 and S8.

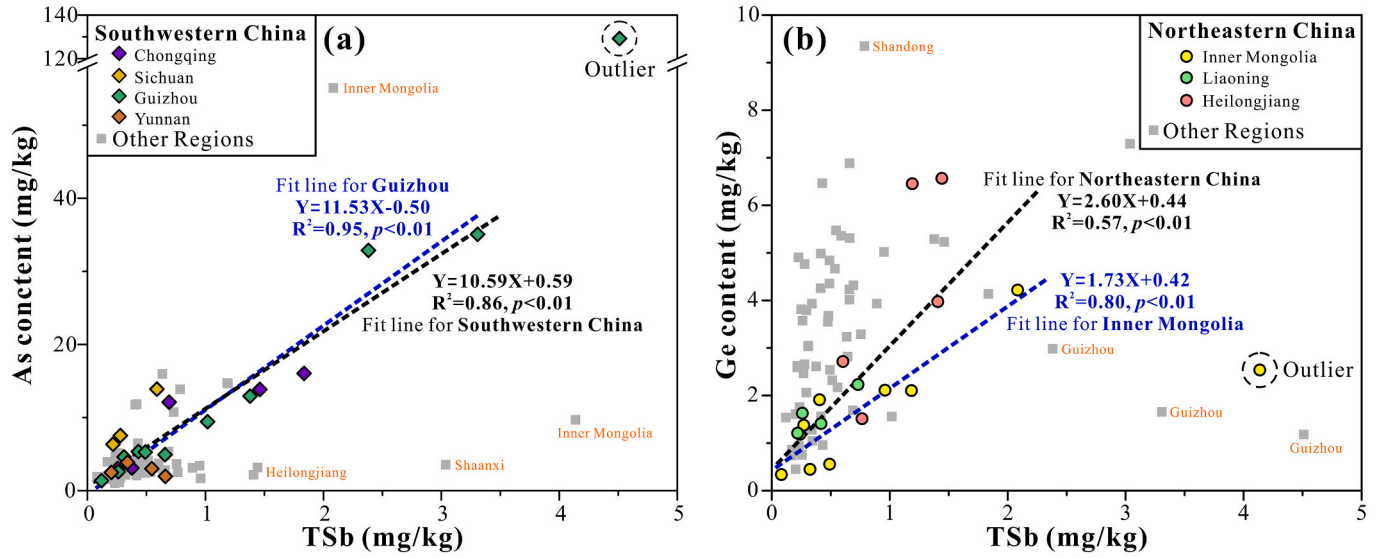

Fig. 6. Correlations between (a) TSb and arsenic (As) content in coal from SW China and (b) TSb and germanium (Ge) content in coal from NE China.

occurrence of hydrothermal Sb in coal from NE China (Sun et al., 2014). In terms of trace elements, TSb significantly correlates with germanium (Ge) contents in coal from NE China ($R^2 = 0.57$, $p < 0.01$, *t*-test) and from Inner Mongolia ($R^2 = 0.80$) (Fig. 6b). Germanium is not incorporated in the minerals in coal, but ~100% is associated with organic matter (Dai et al., 2021). In NE China, Ge-rich coal seams have been identified. The enrichment of Ge in coal has been found to be associated with granites in the vicinity of these seams, where Ge was leached out by atmospheric precipitation and entered the coal (Dai et al., 2015a; Liu et al., 2021b). Similar to Ge, Sb can also be leached from Sb-bearing geological bodies and then enriched in coal via adsorption (Karayiğit et al., 2017; Qi et al., 2007; Seredin, 2003). Coal is a strong sorbent because it contains large amounts of organic matter, Fe-Mn oxides, clay minerals, etc., effectively trapping Sb from the leaching solution (Finkelman et al., 2019; He et al., 2019; He et al., 2012). In addition, framboidal pyrite was observed in coal from Inner Mongolia (Fig. S6e, f). Continental coal may contain syngenetic pyrite through the supply of sulfate from subsurface/surface water (Kortenski and Kostova, 1996; Siavalas et al., 2009), reflecting the potential influence of continental water on trace elements in coal from NE China. The same sources of Sb and Ge in coal have been widely reported (Qi et al., 2007; Seredin, 2003). Qi et al. (2007) compared the major and trace elements in Ge-bearing coal vs. sandstone and lignite in Inner Mongolia and concluded that >90 % of Sb in coal was transferred into the coal seam by leaching solution. There is also a significant correlation ($R^2 = 0.9$) between Ge and Sb in coal from the Khankai Massif, Russia, and their occurrence is mainly associated with organic matter in coal. Their occurrence in coal is linked to the circulation of mixed solutions of groundwater and volcanic hydrothermal fluid (Seredin, 2003). In summary, Sb in coal from NE China is mainly enriched from regional Sb-bearing leaching solutions by adsorption processes (Fig. 8b).

3.3.3. Northern China (region C)

Coal from N China was mainly formed in the continental environment during C_2–P_1 (China National Administration of Coal Geology, 2016; Li et al., 2017). The TSb significantly correlates with ash yield (R^2

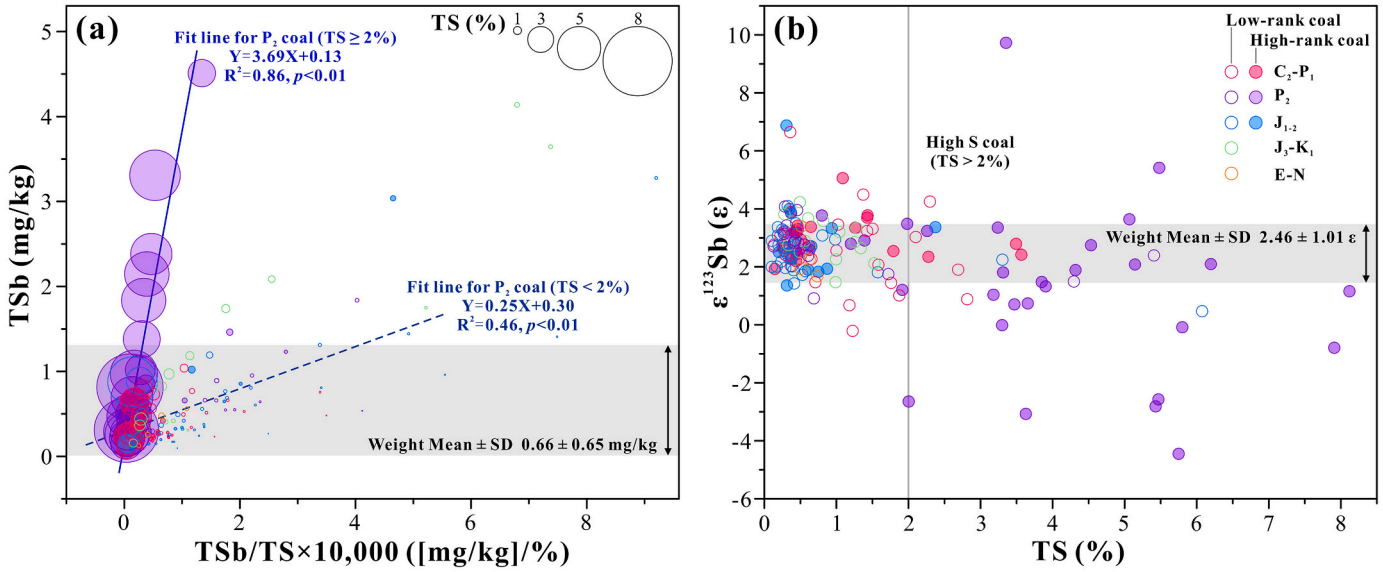

Fig. 7. TSb/TS × 10,000 vs. (a) TSb and (b) ε^{123}Sb. The value of TS is presented with circles of different sizes. High-rank coal (anthracite and bituminous coal) and low-rank coal (subbituminous coal and lignite) are represented by filled circles and hollow circles, respectively.

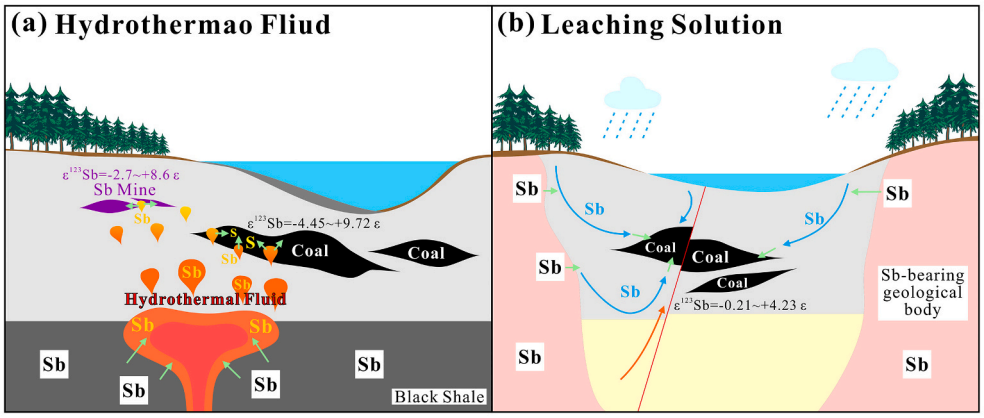

Fig. 8. Schematic diagram of the enrichment processes of Sb in Sb-rich coal from China. Antimony enrichments in coal are affected by (a) hydrothermal fluid and (b) leaching solution.

= 0.33, $p < 0.01$, *t*-test, Fig. S8a) and titanium (Ti) content ($R^2 = 0.28$, $p < 0.01$, *t*-test, Fig. S8b) in coal. The lithophile element Ti in coal is mainly bound to silicates, which are contributed by terrigenous material such as ash in coal (Dai et al., 2021; Finkelman et al., 2018). In addition, vanadium (V) is mainly related to clay in coal, and its content also positively correlates with TSb in C_2–P_1 coal ($R^2 = 0.51$, $p < 0.01$, *t*-test, Fig. S8c) (Dai et al., 2021). Together, these results indicate that terrigenous material is a source of Sb in coal from N China. The TSb also correlates positively with zinc (Zn) content ($R^2 = 0.42$, $p < 0.01$, *t*-test) and As content ($R^2 = 0.50$, $p < 0.01$, *t*-test) in C_2–P_1 coal (Fig. S8d, e). Similar to the other chalcophile elements (e.g., As), the content of Zn is also higher in the bituminous coals than in the low ranked coal, indicating that the geological process in postsedimentary periods plays a leading role in the occurrence of Zn in coal (Finkelman et al., 2018). Both Zn and As mainly exist in the form of sulfides (sphalerite and arsenopyrite) in coal, which are related to hydrothermal fluid (Dai et al., 2021; Finkelman et al., 2018). In addition, the circum-zero Δ^{199}Hg (Fig. 5a) also indicates that hydrothermal fluid affected the C_2–P_1 coal from N China (Sun et al., 2014). However, the relatively stable North China Craton and non-Sb-rich hydrothermal activity resulted in a TSb of only 0.42 ± 0.22 mg/kg (1SD) in coal (Mao et al., 2005), which is obviously different from SW China (region A). This indicates that it is difficult to form Sb-rich coal without Sb-bearing geological bodies to supply Sb to hydrothermal fluid. In conclusion, the origins of Sb in coal from N China are terrigenous materials and hydrothermal fluid.

3.3.4. *Northwestern China (region D)*

Coal from NW China was mainly formed in inland lake basins during J_{1-2} (Li et al., 2017). The TSb in coal positively correlates with TS ($R^2 = 0.20$, $p < 0.05$, *t*-test, Fig. S9a) and thallium (Tl) content ($R^2 = 0.59$, $p < 0.01$, *t*-test, Fig. S9b) in this region. Thallium in coal has been confirmed to be dominantly associated with sulfides (mainly pyrite) (Dai et al., 2021). Sulfur mainly occurs in the form of pyrite in coal from NW China (Li et al., 2012). Framboidal and veined pyrites filled in fissures were both observed in coal from NW China (Fig. S6g-j) (Liu et al., 2017; Zhou et al., 2018). Petrography of pyrite indicates that coal from NW China may face superimposed impacts of the hydrothermal fluid and leaching solution. The mixing of leaching solution may cause a negative Δ^{199}Hg in coal (Fig. 5a) (Sun et al., 2014). In addition, the significant correlation between TSb and Ge content ($R^2 = 0.69$, $p < 0.01$, *t*-test) in J_{1-2} coal (Fig. S9c) also supports the leachate as the source of Sb. Accordingly, the origin of Sb in coal from NW China could be possible superposition of the leaching solution and hydrothermal fluid.

4. Geochemical and environmental significance

The value of ε^{123}Sb in samples with high-temperature geological processes could have a span of 18 ε for stibnite (−2.7 to +8.6 ε) and 11.3 ε for hydrothermal sulfides (−2.2 to +15.8 ε) (Rouxel et al., 2003; Zhai et al., 2021), which are significantly larger than those in low-temperature supergene samples (3.0 ε for soil, 1.8 ε for stream sediment, 1.8 ε for marine sediment, and 1.7 ε for seawater, Fig. 9) (Rouxel et al., 2003; Sun et al., 2021). In this study, the coal from SW (14.17 ε), N (5.97 ε), and NW China (6.40 ε) was affected by hydrothermal fluids to varying degrees. In comparison, the influence of hydrothermal fluid on the coal from NE China (4.44 ε) was small. Consequently, the range of Sb isotopic composition of the coal could be a criterion to reveal the potential influence of hydrothermal influence. The Sb isotopic composition in stibnite indicates that Sb isotopic fractionation in hydrothermal fluid occurs during mineral precipitation and redox reactions (Wang et al., 2021; Zhai et al., 2021). Similarly, a wide span of ε^{123}Sb values induced by hydrothermal fluid has also been recorded in coal from SW China, which may facilitate future studies of Sb isotope fractionation in hydrothermal systems. There are significant differences in the Sb isotopic composition among coal and other environmental samples, including fly ashes, plants, seawater, soils, and sediments (Fig. 9), reflecting the potential to trace the release of coal Sb into the environment by taking advantage of the Sb isotope signature. Furthermore, the establishment of Sb isotopic fingerprints for coal would minimize the uncertainty of its application for tracing sources of Sb contamination in the supergene eco-environment.

5. Conclusions

The analysis of the origin of Sb in coal across China leads to the following major conclusions:

(1) The ε^{123}Sb ranges from −4.45 to +9.72 ε based on 159 coal samples across China, and the weighted mean of ε^{123}Sb based on coal reserves is 2.46 ± 1.01 ε (1SD).
(2) Coal from SW and NE China has higher TSb than that from the other regions. The prime origins of Sb are the hydrothermal fluid and leaching solution. Antimony sources in coal from N (terrigenous materials and hydrothermal fluid) and NW China (leaching solution and hydrothermal fluid) are multiple. The capture and adsorption of Sb by sulfide, organic matter and various minerals in coal are very important for the enrichment of Sb in coal.
(3) The coal affected by the hydrothermal fluid has a wider range of ε^{123}Sb. This is similar to the ε^{123}Sb in ore-forming hydrothermal fluid recorded by stibnite. Therefore, the Sb isotopic composition in coal has great potential to reveal Sb isotopic fractionation in the hydrothermal system.
(4) The significantly different Sb isotopic compositions among coal and different environmental samples would allow Sb isotope methods to have great prospects in tracing Sb in the supergene eco-environment. Consequently, establishing Sb isotopic fingerprints of coal would minimize the methodic uncertainty.

CRediT authorship contribution statement

Xinyu Li: Conceptualization, Data curation, Formal analysis, Methodology, Visualization, Writing – original draft, Writing – review & editing. **Guangyi Sun:** Conceptualization, Funding acquisition, Project administration, Resources, Writing – review & editing. **Yunjie Wu:** Methodology. **Mengying Zhou:** Methodology. **Zhonggen Li:** Investigation. **Xiangyang Bi:** Methodology. **Jen-How Huang:** Writing – review & editing. **Xinbin Feng:** Project administration, Resources, Writing – review & editing, Funding acquisition.

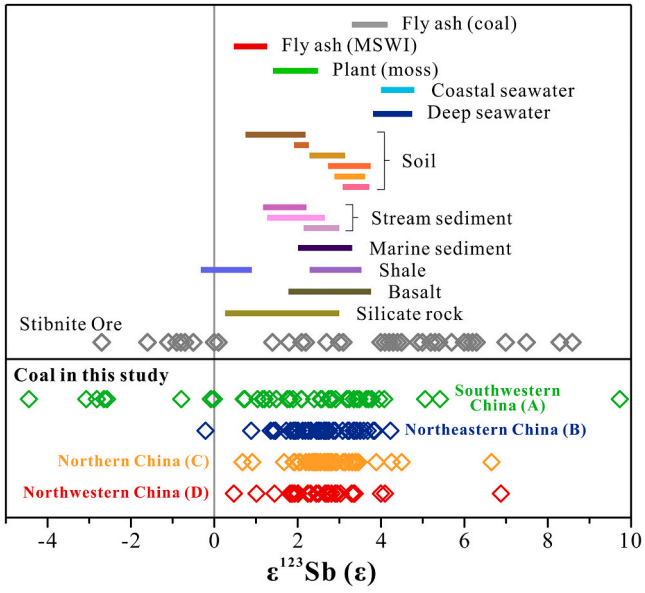

Fig. 9. Antimony isotopic compositions of different environmental and geological materials (Sun et al., 2021; Rouxel et al., 2003; Resongles et al., 2015). Lines represent the mean ± 2SD of ε^{123}Sb. Diamonds represent the ε^{123}Sb distribution of specific samples. MSWI is the abbreviation of municipal solid waste incineration. Different color lines for soil, sediment or shale represent samples of the same type from different regions.

Declaration of Competing Interest

The authors declare that they have no known competing financial interests or personal relationships that could have appeared to influence the work reported in this paper.

Data availability

Data will be made available on request.

Acknowledgments

This work was supported by the Natural Science Foundation of China (grant number 41921004), the Strategic Priority Research Programs of the Chinese Academy of Sciences, the Pan-Third Pole Environment Study for a Green Silk Road (Pan-TPE, XDA2004050201) and the Natural Science Foundation of China (grant number 42277248). We sincerely thank Prof. Shuxiao Wang of Tsinghua University for providing some coal samples.

Appendix A. Supplementary data

Collection and digestion of coal samples; Total Sb content and Sb isotopic analysis; Total sulfur content analysis; Experimental conditions and processing of experimental materials; Weighted calculation of total Sb content and ε^{123}Sb in coal from China. Supplementary data to this article can be found online at [https://doi.org/10.1016/j.coal.2022.104165].

References

ASTM, 2020. ASTM D3174–12(2018)e1: Standard Test Method for Ash in the Analysis Sample of Coal and Coke from Coal. West Conshohocken, PA, ASTM International.
ASTM, 2021. ASTM D388-19a: Standard Classification of Coals by Rank. West Conshohocken, PA, ASTM International.
Bai, X., Li, W., Chen, Y., Jiang, Y., 2007. The general distributions of trace elements in Chinese coals. Coal Qual. Technol. 1, 1–4 (In Chinese with English abstract).
Berner, R.A., 1984. Sedimentary pyrite formation: an update. Geochim. Cosmochim. Acta 48, 605–615.

Biswas, A., Blum, J.D., Bergquist, B.A., Keeler, G.J., Xie, Z., 2008. Natural mercury isotope cariation in coal deposits and organic soils. Environ. Sci. Technol. 42, 8303–8309.
BP, 2020. Statistical Review of World Energy, 69th edition., pp. 44–47
China National Administration of Coal Geology, 2016. China National Administration of Coal Geology, China Occurrence Regularity of Coal Resources and Resource Evaluation. Science Press, Beijing, pp. 44–84 (In Chinese).
Chou, C.-L., 2012. Sulfur in coals: a review of geochemistry and origins. Int. J. Coal Geol. 100, 1–13.
Cutter, G.A., Cutter, L.S., 1998. Metalloids in the high latitude North Atlantic Ocean: sources and internal cycling. Mar. Chem. 61, 25–36.
Dai, S., Ren, D., Tang, Y., Yue, M., Hao, L., 2005. Concentration and distribution of elements in late Permian coals from western Guizhou Province, China. Int. J. Coal Geol. 61, 119–137.
Dai, S., Zeng, R., Sun, Y., 2006. Enrichment of arsenic, antimony, mercury, and thallium in a late Permian anthracite from Xingren, Guizhou, Southwest China. Int. J. Coal Geol. 66, 217–226.
Dai, S., Ren, D., Chou, C.-L., Finkelman, R.B., Seredin, V.V., Zhou, Y., 2012a. Geochemistry of trace elements in Chinese coals: a review of abundances, genetic types, impacts on human health, and industrial utilization. Int. J. Coal Geol. 94, 3–21.
Dai, S., Wang, X., Seredin, V.V., Hower, J.C., Ward, C.R., O'Keefe, J.M.K., Huang, W., Li, T., Li, X., Liu, H., Xue, W., Zhao, L., 2012b. Petrology, mineralogy, and geochemistry of the Ge-rich coal from the Wulantuga Ge ore deposit, Inner Mongolia, China: New data and genetic implications. Int. J. Coal Geol. 90-91, 72–99.
Dai, S., Zhang, W., Ward, C.R., Seredin, V.V., Hower, J.C., Li, X., Song, W., Wang, X., Kang, H., Zheng, L., Wang, P., Zhou, D., 2013. Mineralogical and geochemical anomalies of late Permian coals from the Fusui Coalfield, Guangxi Province, southern China: Influences of terrigenous materials and hydrothermal fluids. Int. J. Coal Geol. 105, 60–84.
Dai, S., Wang, P., Ward, C.R., Tang, Y., Song, X., Jiang, J., Hower, J.C., Li, T., Seredin, V. V., Wagner, N.J., Jiang, Y., Wang, X., Liu, J., 2015a. Elemental and mineralogical anomalies in the coal-hosted Ge ore deposit of Lincang, Yunnan, southwestern China: Key role of N2–CO2-mixed hydrothermal solutions. Int. J. Coal Geol. 152, 19–46.
Dai, S.F., Seredin, V.V., Ward, C.R., Hower, J.C., Xing, Y.W., Zhang, W.G., Song, W.J., Wang, P.P., 2015b. Enrichment of U-Se-Mo-Re-V in coals preserved within marine carbonate successions: geochemical and mineralogical data from the late Permian Guiding Coalfield, Guizhou, China. Mineral. Deposita 50, 159–186.
Dai, S., Hower, J.C., Finkelman, R.B., Graham, I.T., French, D., Ward, C.R., Eskenazy, G., Wei, Q., Zhao, L., 2020. Organic associations of nonmineral elements in coal: a review. Int. J. Coal Geol. 218, 103347.
Dai, S., Finkelman, R.B., French, D., Hower, J.C., Graham, I.T., Zhao, F., 2021. Modes of occurrence of elements in coal: a critical evaluation. Earth-Sci. Rev. 222, 103815.
Filella, M., Belzile, N., Chen, Y.W., 2002. Antimony in the environment: a review focused on natural waters I. Occurrence. Earth-Sci. Rev. 57, 125–176.
Finkelman, R.B., 1994. Modes of occurrence of potentially hazardous elements in coal: levels of confidence. Fuel Process. Technol. 39, 21–34.
Finkelman, R.B., Palmer, C.A., Wang, P., 2018. Quantification of the modes of occurrence of 42 elements in coal. Int. J. Coal Geol. 185, 138–160.
Finkelman, R.B., Dai, S., French, D., 2019. The importance of minerals in coal as the hosts of chemical elements: a review. Int. J. Coal Geol. 212, 103251.
GB/T214–2007, 2007. Determination of total sulfur in coal. Issued by the Chinese General Administration of Quality Supervision. Inspection and Quarantine and the Standardization Administration of China, Beijing (in Chinese).
He, M., Wang, X., Wu, F., Fu, Z., 2012. Antimony pollution in China. Sci. Total Environ. 421-422, 41–50.
He, M., Wang, N., Long, X., Zhang, C., Ma, C., Zhong, Q., Wang, A., Wang, Y., Pervaiz, A., Shan, J., 2019. Antimony speciation in the environment: recent advances in understanding the biogeochemical processes and ecological effects. J. Environ. Sci. 75, 14–39.
Hong, Y., Zhang, H., Zhu, Y., Pu, H., Jiang, H., Zeng, Y., Liu, G., 1992. Characteristics of sulfur isotope composition of Chinese coal and sulfur isotope fractionation during coal combustion. Sci. China. Ser. B Chem. 868–873. https://doi.org/10.1360/zb1992-22-8-868 (In Chinese).
Hu, J., Zheng, B., Wang, M., Finkleman, R.B., 2005. Distribution and forming cause of Sulphur in Chinese coals. Coal Convers. 28, 1–6 (In Chinese with English abstract).
Hu, R., Wen, H., Ye, L., Xia, Y., Fan, H., Huang, Y., Zhu, J., Fu, S., 2020. Metallogeny of critical metals in the Southwestern Yangtze Block. Chin. Sci. Bull. 65, 3700–3714 (In Chinese with English abstract).
Karayiğit, A.I., Spears, D.A., Booth, C.A., 2000. Antimony and arsenic anomalies in the coal seams from the Gokler coalfield, Gediz, Turkey. Int. J. Coal Geol. 44, 1–17.
Karayiğit, A.I., Bircan, C., Mastalerz, M., Oskay, R.G., Querol, X., Lieberman, N.R., Türkmen, I., 2017. Coal characteristics, elemental composition and modes of occurrence of some elements in the İsaalan coal (Balıkesir, NW Turkey). Int. J. Coal Geol. 172, 43–59.
Ketris, M.P., Yudovich, Y.E., 2009. Estimations of clarkes for carbonaceous biolithes: World averages for trace element contents in black shales and coals. Int. J. Coal Geol. 78, 135–148.
Kortenski, J., Kostova, I., 1996. Occurrence and morphology of pyrite in Bulgarian coals. Int. J. Coal Geol. 29, 273–290.
Krenev, V.A., Dergacheva, N.P., Fomichev, S.V., 2015. Antimony: resources, application fields, and world market. Theor. Found. Chem. Eng. 49, 769–772.
Li, J., Zhuang, X., Querol, X., Font, O., Moreno, N., Zhou, J., Lei, G., 2012. High quality of Jurassic Coals in the Southern and Eastern Junggar Coalfields, Xinjiang, NW China: Geochemical and mineralogical characteristics. Int. J. Coal Geol. 99, 1–15.
Li, Z., Wang, D., Lv, D., Li, Y., Liu, H., Wang, P., Liu, Y., Liu, J., Li, D., 2017. The geologic settings of Chinese coal deposits. Int. Geol. Rev. 60, 548–578.
Liu, D., Zhou, A., Zeng, F., Zhao, F., Zou, Y., 2017. The petrography, mineralogy and geochemistry of some Cu- and Pb-enriched coals from Jungar Coalfield, Northwestern China. Miner. 8, 5.
Liu, J., Dai, S., Song, H., Nechaev, V.P., French, D., Spiro, B.F., Graham, I.T., Hower, J.C., Shao, L., Zhao, J., 2021a. Geological factors controlling variations in the mineralogical and elemental compositions of Late Permian coals from the Zhijin-Nayong Coalfield, western Guizhou. China. Int. J. Coal Geol. 247, 103855.
Liu, J., Spiro, B.F., Dai, S., French, D., Graham, I.T., Wang, X., Zhao, L., Zhao, J., Zeng, R., 2021b. Strontium isotopes in high- and low-Ge coals from the Shengli Coalfield, Inner Mongolia, northern China: New indicators for Ge source. Int. J. Coal Geol. 233, 103642.
Mao, J., Xie, G., Zhang, Z., Li, X., Wang, Y., Zhang, C., Li, Y., 2005. Mesozoic large-scale metallogenic pulses in North China and corresponding geodynamic settings. Acta Petrol. Sin. 21, 169–188 (In Chinese with English abstract).
Nation Bureau of Statistics of China, 2021. Statistical yearbook of China. Section 9-5 (Accessed 30 July 2022). http://www.stats.gov.cn/tjsj/ndsj/2021/indexch.htm.
Nehlich, O., 2015. The application of sulphur isotope analyses in archaeological research: a review. Earth Sci. Rev. 142, 1–17.
Ni, J.Y., 1997. Composition Character of Sulfur and Trace Elements in Late Permian Coal of Guizhou Province, China. Doctoral Dissertation of Institute of Geochemistry. Chinese Academy of Sciences, Guiyang, China (In Chinese with English abstract).
Peng, J., Hu, R., Jiang, G., 2003. Samarium-Neodymium isotope system of fluorites from the Qinglong antimony deposit, Guizhou Province: constraints on the mineralizing age and ore-forming materials' sources. Acta Petrol. Sin. 19, 785–791 (In Chinese with English abstract).
Qi, H., Hu, R., Zhang, Q., 2007. Concentration and distribution of trace elements in lignite from the Shengli Coalfield, Inner Mongolia, China: Implications on origin of the associated Wulantuga Germanium Deposit. Int. J. Coal Geol. 71, 129–152.
Qi, C., Liu, G., Chou, C.L., Zheng, L., 2008. Environmental geochemistry of antimony in Chinese coals. Sci. Total Environ. 389, 225–234.
Ren, D., Zhao, F., Dai, S., Zhang, J., Luo, K., 2006. Geochemistry of Trace Elements in Coal. Science Press, Beijing, p. 556 (In Chinese).
Resongles, E., Freydier, R., Casiot, C., Viers, J., Chmeleff, J., Elbaz-Poulichet, F., 2015. Antimony isotopic composition in river waters affected by ancient mining activity. Talanta 144, 851–861.
Ronov, A.B., Yaroshevsky, A.A., Migdisov, A.A., 1990. Chemical composition of the Earth's crust and geochemical balance of main elements. Sc. Pub. (House: Nauka, Moscow, p. 192 (In Russian).
Rouxel, O., Ludden, J., Fouquet, Y., 2003. Antimony isotope variations in natural systems and implications for their use as geochemical tracers. Chem. Geol. 200, 25–40.
Seal, R.R., 2006. Sulfur isotope geochemistry of sulfide minerals. Rev. Mineral. Geochem. 61, 633–677.
Seredin, V.V., 2003. Anomalous trace elements contents in the Spetsugli germanium deposit (Pavlovka brown coal deposit) southern Primorye: Communication 1. Antimony. Lithol. Miner. Resour. 38, 154–161.
Shao, L., Zhang, P., Ren, D., Lei, J., 1998. Late Permian coal-bearing carbonate successions in southern China: coal accumulation on carbonate platforms. Int. J. Coal Geol. 37, 235–256.
Sia, S.-G., Abdullah, W.H., 2012. Enrichment of arsenic, lead, and antimony in Balingian coal from Sarawak, Malaysia: Modes of occurrence, origin, and partitioning behavior during coal combustion. Int. J. Coal Geol. 101, 1–15.
Siavalas, G., Linou, M., Chatziapostolou, A., Kalaitzidis, S., Papaefthymiou, H., Christanis, K., 2009. Paleoenvironment of Seam I in the Marathousa Lignite Mine, Megalopolis Basin (Southern Greece). Int. J. Coal Geol. 78, 233–248.
Song, Y., Liu, Z., Gross, D., Meng, Q., Xu, Y., Li, S., 2018. Petrology, mineralogy and geochemistry of the lower cretaceous oil-prone coal and host rocks from the Laoheishan Basin, Northeast China. Int. J. Coal Geol. 191, 7–23.
Spiro, B.F., Liu, J., Dai, S., Zeng, R., Large, D., French, D., 2019. Marine derived 87Sr/86Sr in coal, a new key to geochronology and paleoenvironment: Elucidation of the India-Eurasia and China-Indochina collisions in Yunnan, China. Int. J. Coal Geol. 215, 103304.
Sun, R., Sonke, J.E., Heimburger, L.E., Belkin, H.E., Liu, G., Shome, D., Cukrowska, E., Liousse, C., Pokrovsky, O.S., Streets, D.G., 2014. Mercury stable isotope signatures of world coal deposits and historical coal combustion emissions. Environ. Sci. Technol. 48, 7660–7668.
Sun, R., Sonke, J.E., Liu, G., 2016. Biogeochemical controls on mercury stable isotope compositions of world coal deposits: a review. Earth-Sci. Rev. 152, 1–13.
Sun, G., Wu, Y., Feng, X., Wu, X., Li, X., Deng, Q., Wang, F., Fu, X., 2021. Precise analysis of antimony isotopic composition in geochemical materials by MC-ICP–MS. Chem. Geol. 582, 120459.
Tang, X., Huang, W., 2004. Trace Elements in Chinese Coals, 6-11. The Commercial Press, Beijing, pp. 24–25 (In Chinese).
Tang, D., Yang, Q., Zhou, C., Kang, X., Liu, D., Huang, W., 2000. Study on the relationship between the microenvironment of Late Paleozoic coal forming marshes in North China and the genesis of sulfur in coal. Sci. China Ser. B Chem. 30, 584–591 (In Chinese with English abstract). https://doi.org/10.1360/zd2000-30-6-584.
Taylor, S.R., McLennan, S.M., 1995. The geochemical evolution of the continental crust. Rev. Geophys. 33, 241–265.
Teng, F.Z., Dauphas, N., Watkins, J.M., 2017. Non-traditional stable isotopes: retrospective and prospective. Rev. Mineral. Geochem. 82, 1–26.
Tian, H., Zhou, J., Zhu, C., Zhao, D., Gao, J., Hao, J., He, M., Liu, K., Wang, K., Hua, S., 2014. A comprehensive global inventory of atmospheric Antimony emissions from anthropogenic activities, 1995-2010. Environ. Sci. Technol. 48, 10235–10241.

Tian, C., Zhang, J., Gupta, R., Zhao, Y., Wang, S., 2015. Chemistry, mineralogical, and residence of arsenic in a typical high arsenic coal. Int. J. Miner. Process. 141, 61–67.
Tryst, B.A., Fry, B., 1992. Stable sulphur isotopes in plants: a review. Plant Cell Environ. 15, 1105–1110.
Wang, D., Mathur, R., Zheng, Y., Qiu, K., Wu, H., 2021. Redox-controlled antimony isotope fractionation in the epithermal system: New insights from a multiple metal stable isotopic combination study of the Zhaxikang Sb–Pb–Zn–Ag deposit in Southern Tibet. Chem. Geol. 584, 120541.
White, W.M., 2013. Geochemistry. John Wiley & Sons, Ltd, UK, p. 271.
Wu, G., Zhu, J.-M., Wang, X., Johnson, T.M., Han, G., 2020. High-sensitivity measurement of Cr isotopes by double spike MC-ICP–MS at the 10 ng level. Anal. Chem. 92, 1463–1469.
Xiao, H.-Y., Liu, C.-Q., 2011. The elemental and isotopic composition of sulfur and nitrogen in Chinese coals. Org. Geochem. 42, 84–93.
Xiao, H.Y., Tang, C.G., Zhu, R.G., Wang, Y.L., Xiao, H.W., Liu, C.Q., 2011. Tracing sources of coal combustion using stable sulfur isotope ratios in epilithic mosses and coals from China. J. Environ. Monit. 13, 2243–2249.
Xie, P., Song, H., Wei, J., Li, Q., 2016. Mineralogical characteristics of late permian coals from the Yueliangtian coal mine, Guizhou, Southwestern China. Mineral. 6, 29.
Yan, X., Dai, S., Graham, I.T., French, D., Hower, J.C., 2019. Mineralogy and geochemistry of the Paleogene low-rank coal from the Baise Coalfield, Guangxi Province, China. Int. J. Coal Geol. 214, 103282.
Yin, R., Feng, X., Chen, J., 2014. Mercury stable isotopic compositions in coals from major coal producing fields in China and their geochemical and environmental implications. Environ. Sci. Technol. 48, 5565–5574.
Zhai, D., Mathur, R., Liu, S.-A., Liu, J., Godfrey, L., Wang, K., Xu, J., Vervoort, J., 2021. Antimony isotope fractionation in hydrothermal systems. Geochim. Cosmochim. Acta 306, 84–97.
Zhang, G., Gu, X., 1996. The sulfur isotope compositions and geochemical characteristics of the antimony deposits of main types in China. Miner. Resour. Geol. 13, 172–178 (In Chinese with English abstract).
Zhang, T., Li, C., Sun, S., Hao, X., 2020. Geochemical characteristics of antimony and genesis of antimony deposits in South China. Acta Petrol. Sin. 36, 44–54 (In Chinese with English abstract).
Zheng, B.S., Ding, Z.H., Huang, R.G., Zhu, J.M., Yu, X.Y., Wang, A.M., Zhou, D.X., Mao, D.J., Su, H.C., 1999. Issues of health and disease relating to coal use in southwestern China. Int. J. Coal Geol. 40, 119–132.
Zhou, J., Tian, H., Zhu, C., Hao, J., Gao, J., Wang, Y., Xue, Y., Hua, S., Wang, K., 2015. Future trends of global atmospheric antimony emissions from anthropogenic activities until 2050. Atmos. Environ. 120, 385–392.
Zhou, S., Liu, D., Cai, Y., Karpyn, Z., Yao, Y., 2018. Petrographic controls on pore and fissure characteristics of coals from the Southern Junggar Coalfield, Northwest China. Energ. 11, 1556.
Zhou, W., Zhou, A., Wen, B., Liu, P., Zhu, Z., Finfrock, Z., Zhou, J., 2022. Antimony isotope fractionation during adsorption on aluminum oxides. J. Hazard. Mater. 429, 128317.
Zhu, J.-M., Wu, G., Wang, X., Han, G., Zhang, L., 2018. An improved method of Cr purification for high precision measurement of Cr isotopes by double spike MC-ICP–MS. J. Anal. Atom. Spectrom. 33, 809–821.